

Spectroscopic bulge–disc decomposition: a new method to study the evolution of lenticular galaxies

E.J. Johnston,^{1*} A. Aragón-Salamanca,¹ M.R. Merrifield¹ and A.G. Bedregal^{2,3}

¹*School of Physics and Astronomy, University of Nottingham, University Park, Nottingham, NG7 2RD, UK*

²*Departamento de Astrofísica, Facultad de Ciencias Físicas, Universidad Complutense de Madrid, 28040 Madrid, Spain*

³*Institute for Astrophysics, University of Minnesota, 116 Church Street SE, Minneapolis, MN 55455 USA*

11 November 2018

ABSTRACT

A new method for spectroscopic bulge–disc decomposition is presented, in which the spatial light profile in a two-dimensional spectrum is decomposed wavelength-by-wavelength into bulge and disc components, allowing separate one-dimensional spectra for each component to be constructed. This method has been applied to observations of a sample of nine lenticular galaxies in the Fornax Cluster in order to obtain clean high-quality spectra of their individual bulge and disc components. So far this decomposition has only been fully successful when applied to galaxies with clean light profiles, without contamination from dust lanes etc. This has consequently limited the number of galaxies that could be separated into bulge and disc components. Lick index stellar population analysis of the component spectra reveals that in those galaxies where the bulge and disc could be distinguished, the bulges have systematically higher metallicities and younger stellar populations than the discs. This correlation is consistent with a picture in which S0 formation comprises the shutting down of star formation in the disc accompanied by a final burst of star formation in the bulge. Similarly, a trend was found to exist whereby galaxies with younger stellar populations have higher metallicities. The variation in spatial-fit parameters with wavelength also allows us to measure approximate colour gradients in the individual components. Such gradients were detected separately in both bulges and discs, in the sense that redder light is systematically more centrally concentrated in all components. However, a search for radial variations in the absorption line strengths determined for the individual components revealed that, although they can be sensitively detected where present, they are absent from the vast majority of S0 discs and bulges. The absence of gradients in line indices for most galaxies implies that the colour gradient cannot be attributed to age or metallicity variations, and is therefore most likely associated with varying degrees of obscuration by dust.

Key words: galaxies: elliptical and lenticular – galaxies: evolution – galaxies: formation – galaxies: clusters – galaxies: stellar content

1 INTRODUCTION

The evolution of galaxies in different environments is still poorly understood, as is the relative importance of the different processes involved. Lenticular galaxies (S0s) lie between spirals and ellipticals on the Hubble Sequence, and share many properties with both of these morphologies such as the redder colours and older stellar populations of ellipticals along with the stellar discs of spirals. As a result, S0s are often seen as a transitional phase between spirals and ellipticals, and thus understanding their origins is thought to be a key stage in understanding galaxy evolution. The many influences controlling their evolution are expected to affect the bulges

and discs of these galaxies in different ways, and so the individual study of these components should provide valuable clues as to their evolutionary histories.

Evidence for the evolution of galaxies along the Hubble Sequence with redshift lies in the morphology–density relation for clusters of galaxies. This relation shows that spirals tend to dominate the less-dense outer regions, while the early types tend to lie at the cores of clusters (Dressler 1980), and that the relative fraction of spiral galaxies in clusters decreases toward lower redshifts while the fraction of S0s increases (Dressler et al. 1997). This finding has been supported by studies using larger samples of galaxies, such as Whitmore, Gilmore & Jones (1993), Fasano et al. (2000) and Desai et al. (2007). Similarly, Varela et al. (2004) have also found that late-type spirals are more frequent among iso-

* Email: ppcej@nottingham.ac.uk

lated galaxies, while S0s are more commonly found in denser environments such as galaxy groups and clusters. Many scenarios have been proposed for the transformation of spirals into S0s, mostly focusing on the truncation of star formation within the galaxy followed by passive evolution into an S0. Processes include the removal of the cold disc gas by ram pressure stripping (Gunn & Gott 1972), the removal of the hot halo gas by a process usually called starvation (Larson, Tinsley & Caldwell 1980; Bekki, Shioya & Couch 2002), tidal stripping by galaxy harassment (Moore et al. 1996; Moore, Lake & Katz 1998; Moore et al. 1999), and starbursts triggered by unequal mass galaxy mergers (Mihos & Hernquist 1994) and galaxy–cluster interactions (Merritt 1984; Miller 1986; Byrd & Valtonen 1990).

Since these processes would affect galactic bulges and discs differently, many studies have tried looking for clues to S0 star formation histories by photometric bulge–disc decomposition. The parameters for the bulge and disc can be plotted as the Kormendy Relation (Kormendy 1977), where the effective surface brightness for each component is plotted against its scale length. This generally shows that the surface brightness falls as the scale length increases over a large sample of spirals, but Barway et al. (2009) found that while S0s in the field show this trend, faint cluster S0s do not, instead forming a downward scatter where the effective surface brightness drops significantly at larger scale lengths. This drop is thought to be evidence of transformations induced by environmental effects such as minor mergers, ram pressure stripping or harassment. Barway et al. (2007) also found that in faint S0s the bulge effective radius increases with the disc scale length, while in brighter S0s it decreases with increasing disc scale length. Secular evolution of spirals into lenticulars predicts the former trend since the passive fading of the bulge and disc would conserve their scale lengths, while the latter correlation would be expected from a more turbulent transition. Therefore this variation suggests that lenticulars may have evolved in different ways depending on their environments.

By analysing multi-waveband photometry it is possible to look at the colour differences and gradients within the bulge and disc. Such data can in turn provide information on the star formation histories of these galaxies since higher metallicities and older stellar populations strengthen the redder light from the galaxy. Negative colour gradients have been found in the bulges of S0s (Terndrup et al. 1994; Peletier & Balcells 1996) and spirals (Möllenhoff 2004), showing that the blue light is distributed throughout the bulge while redder light is more concentrated in the centre. In addition to this it has been found that the discs of S0s and spirals are bluer than the bulges (Bothun & Gregg 1990; Peletier & Balcells 1996; Hudson et al. 2010), suggesting that disc galaxies have more recent star formation activity at larger radii (de Jong 1996) or higher metallicities in their nuclear regions (Beckman et al. 1996; Pompei & Natali 1997). These trends indicate the presence of age and metallicity gradients across the galaxies, but fail to provide information on whether it represents a gradient within the individual components, or whether it arises simply from the superposition of varying amounts of bulge and disc light, where each component contains stellar populations of different ages and metallicities. It also leaves open the possibility that the gradients could result from differing amounts of dust extinction at different radii, rather than telling us about spatial variations in the stellar population.

To resolve this ambiguity, we have developed a new method to apply bulge–disc decomposition to long-slit spectroscopy of nearby galaxies. The technique involves dividing the two-dimensional

spectrum into two one-dimensional spectra, one representing purely the bulge light and the other the disc light. This decomposition is achieved by fitting the spatial profile of light at each wavelength with a disc-plus-bulge model in order to ascertain the fraction of the light that should be ascribed to each component at that wavelength. By repeating this analysis at every wavelength, the individual spectra of bulge and disc can be constructed. These “clean” spectra can then be analysed for their ages and metallicities, as well as any gradients in these quantities, to determine the sequence of events in the formation of S0 galaxies.

This paper is intended to present the new method, and give an indication of its potential by applying the technique to a relatively small sample of S0s from the Fornax Cluster. Section 2 describes the Fornax data sample and observations. Section 3 presents the development of the method, and its initial application to the Fornax Cluster data. Section 4 analyses these results in terms of the stellar populations in the bulges and discs of these galaxies, and Section 5 looks at their colour gradients. Section 6 searches for any corresponding gradients in line indices and hence ages or metallicities. Finally, our conclusions are presented in Section 7.

2 THE DATA SAMPLE

The initial sample on which we are testing this new method comprises the nine lenticular galaxies in the Fornax Cluster, as classified by Kuntschner (2000), with inclinations above 60 degrees and luminosities in the range $-22.3 < M_B < -17.3$. The data were obtained using the 8.2 m Antu/VLT between 2002 October 2 and 2003 February 24 with the FORS2 instrument in long-slit spectroscopy mode. The slit was aligned with the major axis of each galaxy, and was set to 0.5 arcsec wide and 6.8 arcmin in length. For all galaxies except NGC 1316, the centre of the galaxy was placed half way along the slit in order to obtain information along the entire length of the major axis; NGC 1316 is the largest galaxy in the sample, and it was necessary to offset it along the slit in order to cover sufficient sky for background subtraction. The standard resolution collimator was used in the unbinned readout mode, giving a spatial scale of $0.125 \text{ arcsec pixel}^{-1}$, and the GRIS1400V+18 grism gave a dispersion of $0.318 \text{ \AA pixel}^{-1}$ over a wavelength range of $4560 \leq \lambda \leq 5860 \text{ \AA}$. By analysing arc lines, the spectral resolution was found to be $\sim 4 \text{ pixels FWHM}$, which corresponds to a velocity resolution of $\sim 73 \text{ km s}^{-1}$ FWHM or a velocity dispersion of $\sim 31 \text{ km s}^{-1}$. Details of the data reduction are given in Bedregal et al. (2006).

3 SPECTROSCOPIC BULGE–DISC DECOMPOSITION

Conventional photometric one-dimensional bulge–disc decomposition of galaxies involves measuring the luminosity along the galaxy’s major axis. The decomposition is obtained by plotting the luminosity against radius, and fitting model bulge and disc components to this profile. The disc is generally modeled as an exponential,

$$I_D(R) = I_{D0} \exp(-R/R_0), \quad (1)$$

where I_{D0} is the central surface brightness of the disc and R_0 is the disc scale length (Freeman 1970). Similarly, the light profile of the bulge can be approximated by a de Vaucouleurs profile,

$$I_B(R) = I_{Be} \exp \left\{ -7.669 \left[(R/R_e)^{1/4} - 1 \right] \right\}, \quad (2)$$

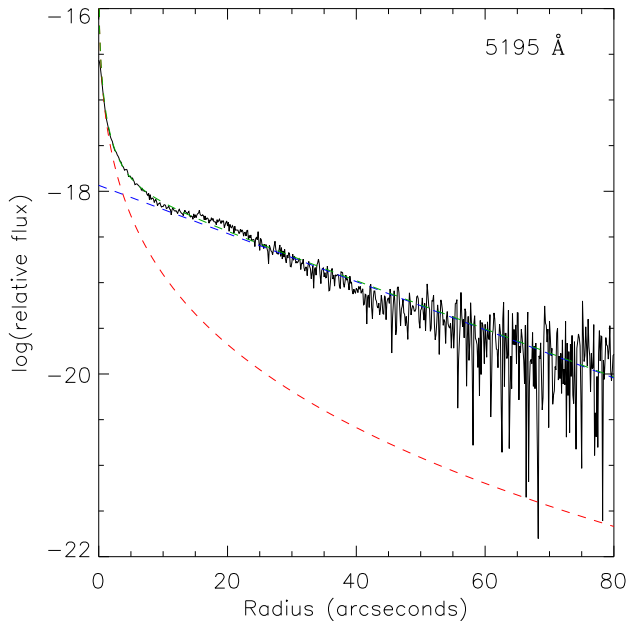


Figure 1. The light profile of NGC 1375 at 5195 Å in black with the best fit model in green, comprising the sum of a disc (blue line) and bulge (red line) components.

where R_e is the bulge effective radius and I_{Be} is the bulge effective surface brightness (de Vaucouleurs 1953). For a two-dimensional spectrum we can apply exactly the same method to each individual wavelength in the data. For example, Fig. 1 shows the light profile along the major axis of NGC 1375 at 5195 Å, together with the best fit achieved using a de Vaucouleurs bulge and exponential disc.

The only complication here is accounting for the velocity dispersion and radial velocity, where the velocity dispersion of the galaxy decreases at larger radii, while the rotational velocity red- or blue-shifts the spectra at larger radii relative to that from the centre of the galaxy. Therefore, before fitting the light profile at each wavelength, the two-dimensional spectrum must be corrected such that each spectral feature has the same velocity dispersion and radial velocity, thus ensuring that the light profiles for each wavelength bin measures the light from the same point on the rest-frame spectrum at all radii. Extra care must be taken with this correction when a bar is present within the galaxy to account for its kinematics. The velocity dispersion was corrected by convolving the spectrum from each spatial location with the appropriate Gaussian to bring it up to the maximum value measured within that galaxy. The rotational velocity was then corrected by cross correlation, where the shift in the wavelength of the spectral features at each location was measured relative to those in the peak spectrum. In order to minimise the noise in these shift measurements, a rolling average was applied to the shifts for each spectrum until the radius where the noise dominated the results, at which point the final reliable shift was applied to the remaining rows. This gave a smooth velocity curve from which the necessary shift could be calculated. Since the two-dimensional spectra cover the entire length of the major axis in all but one galaxy in the sample, the two halves of each galaxy spectrum, i.e. the two semi-major axes, were analysed separately. This duplication was useful to ensure the results were reproducible for each galaxy, and can also provide information on spatial asymmetries within the galaxies.

Once this velocity alignment has been carried out, we can per-

form the bulge–disc decomposition at all wavelengths. By way of illustration, Fig. 2 shows a small section of the models produced for NGC 1381 of the bulge, disc and composite galaxy, as derived by fitting the spatial profile of the two-dimensional spectrum (also shown) wavelength by wavelength. In each profile, the central few arcseconds were masked out prior to fitting in order to eliminate the effects of seeing, so the peaks of the bulge and disc spectra at very small radii in Fig. 2 were not used in the fit. Additionally, the light profiles of each galaxy were also checked by eye to ensure that the exponential parts most likely represented the disc rather than the spheroid. This was found to be the case in all the galaxies that were decomposed successfully. The results for the bulge effective radius and disc scale length for each galaxy from the decomposition are given in Appendix A. These were compared to the photometric results of (Bedregal et al. 2006) derived from the Two-Micron All-Sky Survey (2MASS) K-band images of these galaxies, and were found to be reasonably consistent considering the limited model used in this study.

The total luminosity of the bulge and disc at each wavelength can then be calculated by simple integration, using the standard results that

$$L_B(\lambda) = 7.22\pi I_e(\lambda) R_e^2(\lambda) \quad (3)$$

for the bulge, and

$$L_D(\lambda) = I_0(\lambda) R_0^2(\lambda) \quad (4)$$

for the disc, where we have now made the dependence on wavelength, λ , of the various fitted parameters explicit. These quantities are simply the modeled spectra of the integrated light from the separate bulge and disc components. For example, Fig. 3 shows the spectra derived in this way for NGC 1375. The high signal-to-noise ratio of the spectra obtained using this integrated light approach is immediately apparent, such that one can see that both the H β line and the magnesium triplet appear stronger in the bulge than in the disc; since these features are used as age and metallicity indicators respectively, this difference already hints that the bulge contains younger stars with a higher metallicity than the disc in this galaxy, and we will make a more quantitative assessment of this impression in Section 4.

Application of this technique to the full sample of galaxies described in Section 2 revealed the kind of data required to implement this analysis successfully. In fact, of the nine galaxies, only two (NGC 1381 and NGC 1375) could be reliably decomposed into bulge and disc spectra in this manner. A further three galaxies (IC 1963, ESO 358-G006 and ESO 359-G002) were found by Bedregal et al. (2006) to have very compact bulges and therefore to be disc dominated from very small radii, making it impossible to determine a reliable bulge model. For these systems a disc spectrum was extracted by assuming that the bulge light was negligible outside of the central masked region, and just fitting a disc component. In two further cases (NGC 1380 and NGC 1316) we found that although the spectra could be decomposed into bulge and disc components, the resulting model did not reproduce the original two-dimensional spectrum at all well. Images of these galaxies clearly show the presence of major-axis dust lanes in both cases, which would affect the light profile, and it has also been suggested by Caon, Capaccioli & D’Onofrio (1994) that NGC 1316 is a merger remnant, which would complicate its light profile and therefore make it unsuitable for fitting a de Vaucouleurs bulge and exponential disc. The final two spectra (NGC 1380A and ESO 358-G059) could not be decomposed as their light profiles were again too complex for the current simple model. We have therefore as-

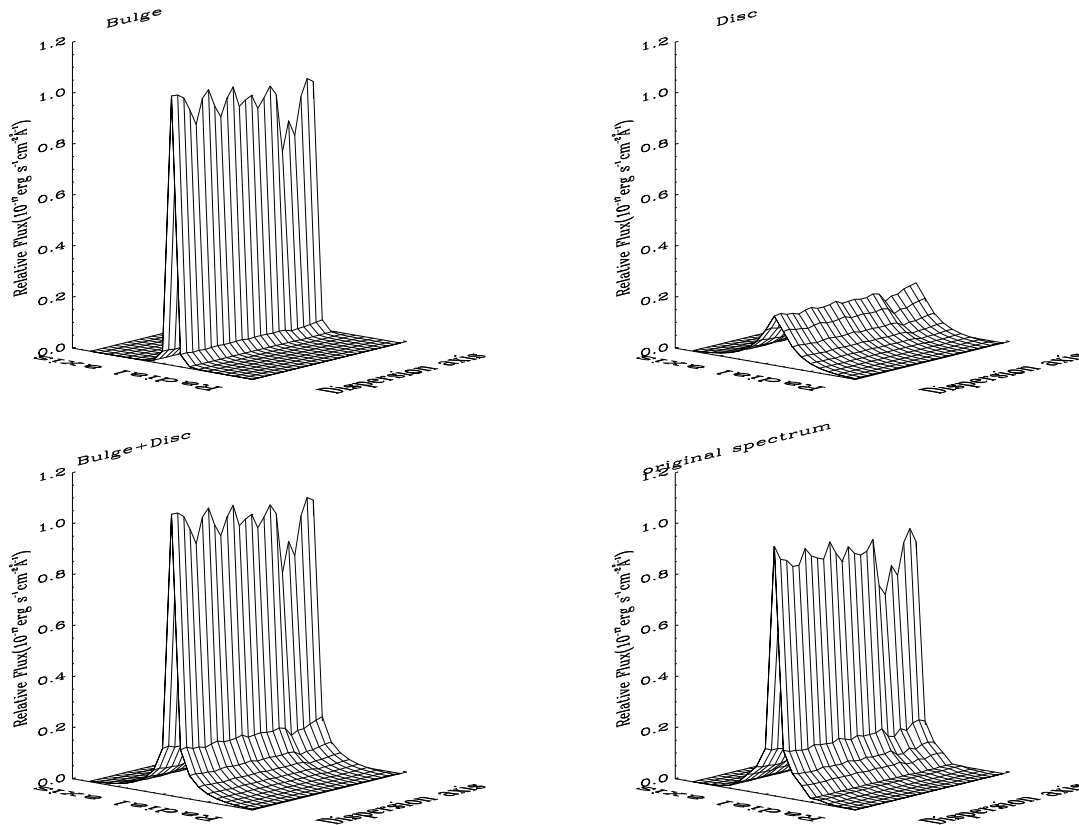


Figure 2. A section of the two-dimensional spectra for the bulge, disc and composite models, and the original spectrum of NGC 1381, showing how the light profile varies with wavelength. The data have been binned such that each step in the radial direction is $12.5''$, and in the dispersion direction is 6.6\AA . The wavelength range covered is between 5085\AA and 5243\AA , increasing towards the right of the diagrams. Note that the peak values of the bulge and composite spectra have been reduced by a factor of four in order to allow them to be plotted on the same scale as the original spectrum.

certained that this approach works best in systems where both components are well resolved, and where there is little indication of complicating issues like strong dust lanes or extra components such as bars. Fortunately, comparison between the original two-dimensional spectrum and the model offers a useful *a posteriori* check on the impact of such additional factors.

4 STELLAR POPULATIONS

In the integrated light spectrum of a galaxy, the strength of the various absorption lines provides information on the underlying stellar population, with hydrogen lines primarily associated with its age, while magnesium and iron lines constrain its metallicity. In order to obtain quantitative estimates of age and metallicity, these line indices can be compared to those predicted by simple stellar population (SSP) models that have been created using stellar libraries of the same spectral resolution as the data. In this study, the SSP models used are those of Vazdekis et al. (2010), which uses the MILES stellar library (Sánchez-Blázquez et al. 2006). The library spectra have a resolution of $\sim 58.4 \text{ km s}^{-1}$, and are matched to the spectral resolution of the data by convolving the stellar spectra with a Gaussian of the appropriate dispersion. These data are available as a web-based tool¹ that allows the user to modify the library spectra

to the resolution and redshift of their observations, and therefore obtain tuned SSP models for their data.

The line strength indices in the data were measured using the INDEXF software of Cardiel (2007), which uses the Lick/IDS index definitions to calculate a pseudo-continuum over each absorption feature based on the level of the spectrum in bands on either side (Worthey et al. 1994; Worthey & Ottaviani 1997). The strength of the spectral feature was then measured relative to this pseudo-continuum, and the uncertainty estimated from the propagation of random errors and the effect of uncertainties in the radial velocity.

As one further slight complication, Bedregal et al. (2008) found that the galaxies in this sample show traces of emission in the $H\beta$ line which would reduce the absorption-line strength of this line and skew the results to older ages. To correct for this contamination, González (1993) identified that the ratio between the equivalent widths of the $[\text{OIII}]_{\lambda 5007}$ and $H\beta$ emission features is around 0.7 in the brightest ellipticals. A later study by Trager et al. (2000) found the ratio to vary between 0.33 to 1.25 with a mean value of 0.6. This mean value was used here to estimate the level of emission correction necessary for the $H\beta$ index, using

$$\Delta(H\beta) = 0.6 \times \text{EW}[\text{OIII}]_{\lambda 5007}, \quad (5)$$

where the $[\text{OIII}]_{\lambda 5007}$ index was measured from the residual spectrum obtained by subtracting the best combinations of stellar templates from the original galaxy spectrum. These fits were

¹ <http://miles.iac.es/>

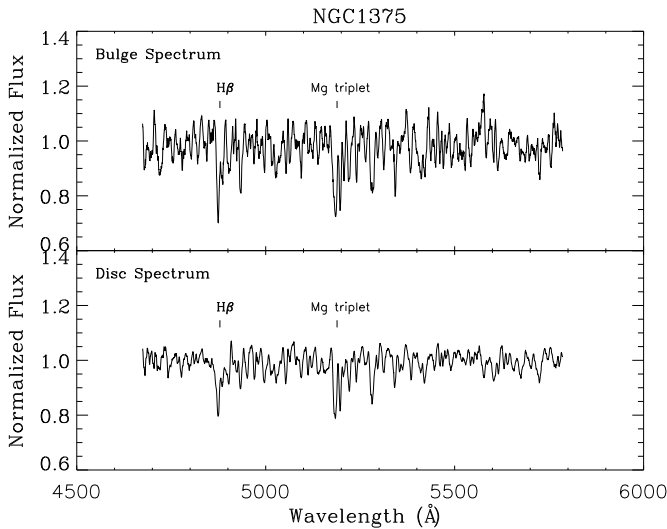


Figure 3. The decomposed one-dimensional bulge and disc spectra for NGC 1375.

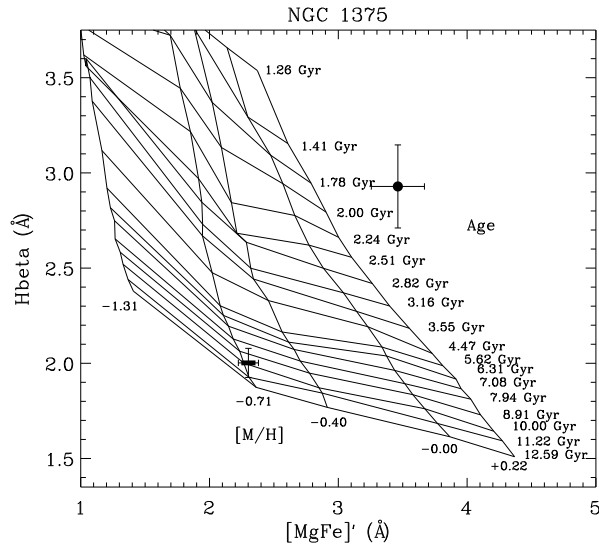


Figure 4. Example of the bulge and disc data for NGC 1375 with the Vazdekis et al. (2010) SSP model for the bulge kinematics over-plotted. $H\beta$ is the age indicator while $[MgFe]'$ is the metallicity indicator. The circle represents the bulge while the rectangle corresponds to the disc value. The error bars represent the statistical uncertainties.

achieved using the Penalized Pixel Fitting method (PPXF) of Cappellari & Emsellem (2004), which uses the MILES stellar library to model the line-of-sight velocity distribution as a Gaussian with a series of Gauss-Hermite polynomials. For this sample, the $H\beta$ corrections were never more than 24% of the $H\beta$ index, with the majority being less than 10%, so any residuals from the approximate nature of this correction are unlikely to compromise the results significantly. The PPXF code also used the stellar library to measure the line of sight velocity and velocity dispersion for each decomposed spectrum, which could then be used to tune the SSP models. These values are also given in Appendix A.

Having measured and corrected the observed line strengths,

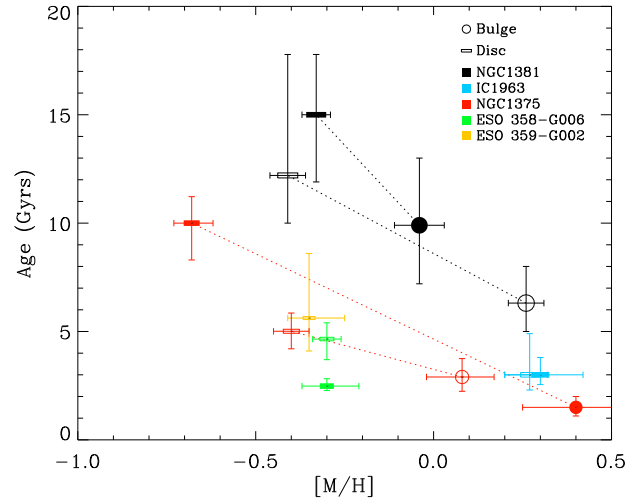


Figure 5. Age versus metallicity for the decomposed spectra. Each galaxy is represented by a different colour, with circles and rectangles corresponding to bulges and discs respectively. Dotted lines join the bulge and disc of the same galaxy. The size of each symbol reflects the luminosity of the galaxy (Madore et al. 1999). The filled and open symbols are used to show the results from the two semi-major axes in each galaxy, where both could be measured.

SSP models were created for each decomposed spectrum and plotted using $H\beta$ and $[MgFe]'$ as the age and metallicity indicators respectively, where the latter was chosen due to its negligible dependence on the α -element abundance (González 1993; Thomas, Maraston & Bender 2003). As an example, Fig. 4 shows the indices derived for the bulge and disc spectra of NGC 1375, together with the grid of predictions for SSP models of differing ages and metallicities corrected to the velocity dispersion of this galaxy, from which one can read off estimates of the relative age and metallicity for the data. Since these measurements were obtained from spectra representing the integrated light over the full bulge and disc, they correspond to the global, luminosity-weighted values for age and metallicity for each component. The errors shown reflect the statistical uncertainties outlined above. Clearly in this case the bulge is inferred to be young and metal rich, while the disc is old and metal poor.

Figure 5 shows the results of this analysis applied to all galaxies in the sample. Where both were observed, we show the two sides of each galaxy separately, principally as a test of the reproducibility of the results. Dotted lines join the bulges and discs derived from the same side of the same galaxy, while points corresponding to different halves of the major axis of the same galaxy share the same colour. In the few cases where the index measurements lay outside of the SSP model grids, such as in Fig. 4, the metallicities were estimated by using an extrapolation method. Due to the uncertainties already mentioned, and the fact that different SSP models would give different grids, it is important to consider the results in Fig. 5 as constraining the relative ages and metallicities within the data set as opposed to their absolute values. The errors shown on the data points correspond to the statistical errors given in Fig. 4 plus interpolation errors, while a more realistic measure of the uncertainties can be obtained by comparing the results for each half of the major axis of each galaxy, as represented by closed and filled symbols. It can be seen that both within individual galaxies and viewing the data set as a whole, there is clearly a trend

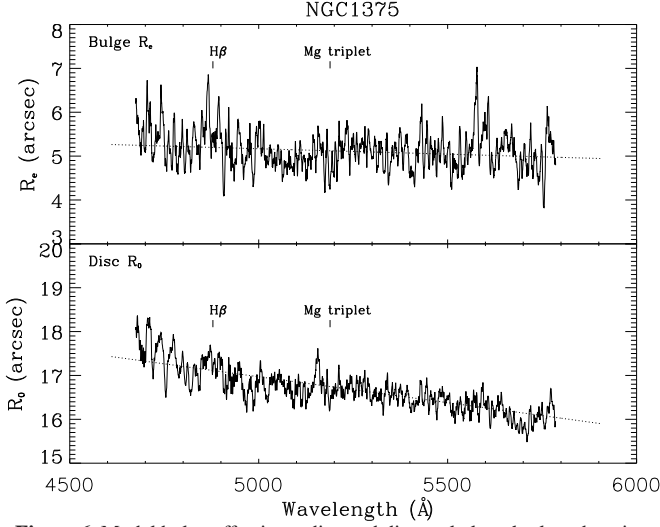


Figure 6. Model bulge effective radius and disc scale length plotted against wavelength for NGC1375. A strong negative gradient can be seen in the disc scale-length, corresponding to a negative colour gradient across the disc, while the gradient in the bulge is much weaker.

in the sense that the bulges are systematically younger and more metal rich than the discs.

5 COLOUR GRADIENTS

As well as estimating the global ages and metallicities of the bulges and discs, this spectral decomposition method also provides an approximate measure of any gradients in the properties of components. Specifically, if there were a colour gradient in a component, such that, say, red light was more centrally concentrated than blue light, then the characteristic size-scale of the component would be smaller in red light than in blue light. Because we determine the length-scales of both disc and bulge as a function of wavelength, it is straightforward to see whether any such gradients exist. For example, Fig. 6 shows the bulge and disc length-scales across the range of wavelengths observed for NGC 1375. In both cases, there is a negative gradient, indicating that the centre of each component is redder than its outer parts, although the effect is clearly stronger in the disc than the bulge.

In order to quantify this effect in terms of more conventional colour gradients, we can calculate the bulge effective radius and the disc scale-length at the central wavelengths of the B and V band filters from the Johnson-Cousins system [4450 Å and 5510 Å respectively (Bessell 1990)]. For the bulge, the ratio of light in the B -band to that in the V -band is given by

$$\frac{I_B}{I_V} = \left(\frac{I_{eB}}{I_{eV}} \right) \exp \left\{ -7.67 \left[\left(\frac{1}{R_{eB}} \right)^{1/4} - \left(\frac{1}{R_{eV}} \right)^{1/4} \right] R^{1/4} \right\}, \quad (6)$$

or, in magnitudes,

$$B - V = \text{const} - 2.5 \log_{10} \left(\frac{I_{eB}}{I_{eV}} \right) + 19.18 \left(\frac{1}{R_{eB}^{1/4}} - \frac{1}{R_{eV}^{1/4}} \right) R^{1/4} \log_{10} e. \quad (7)$$

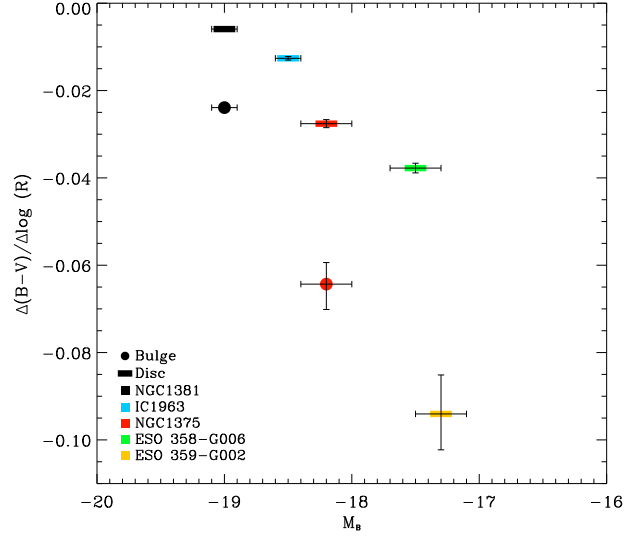


Figure 7. The colour gradients in the bulges (circles) and discs (rectangles) of each galaxy against the galaxy's absolute B -band magnitude. The colours of the points are as in Fig. 5.

Differentiating with respect to $R^{1/4}$, we find

$$\frac{d(B - V)}{d(R^{1/4})} = 8.3 \left(\frac{1}{R_{eB}^{1/4}} - \frac{1}{R_{eV}^{1/4}} \right). \quad (8)$$

This equation can then be integrated out from the centre to any radius, to obtain a change in colour,

$$(B - V)_R - (B - V)_0 = 8.3 \left(\frac{1}{R_{eB}^{1/4}} - \frac{1}{R_{eV}^{1/4}} \right) R^{1/4}. \quad (9)$$

As a characteristic radius, we set $R = R_{eV}$ in Equation (9), and then divide by $\log R_{eV}$ to create an appropriate gradient quantity.

We can also obtain a set of analogous equations in order to define a gradient in the disc:

$$\frac{I_B}{I_V} = \left(\frac{I_{0B}}{I_{0V}} \right) \exp \left[- \left(\frac{1}{R_{0B}} - \frac{1}{R_{0V}} \right) R \right]; \quad (10)$$

$$B - V = \text{const} - 2.5 \log_{10} \left(\frac{I_{0B}}{I_{0V}} \right) + 2.5 \left(\frac{1}{R_{0B}} - \frac{1}{R_{0V}} \right) R \log_{10} e; \quad (11)$$

$$\frac{d(B - V)}{d(R)} = 1.09 \left(\frac{1}{R_{0B}} - \frac{1}{R_{0V}} \right); \quad (12)$$

$$(B - V)_R - (B - V)_0 = 1.09 \left(\frac{1}{R_{0B}} - \frac{1}{R_{0V}} \right) R. \quad (13)$$

The colour gradients obtained from these formulae using the observed variation in scale-length with wavelength for each component of each galaxy are shown in Fig. 7. In all cases, the colour gradients are negative, indicating that the centres are redder than the outskirts, in both bulge and disc components. There also appears to be a trend that the gradients are stronger in fainter galaxies. The range of values obtained are directly comparable

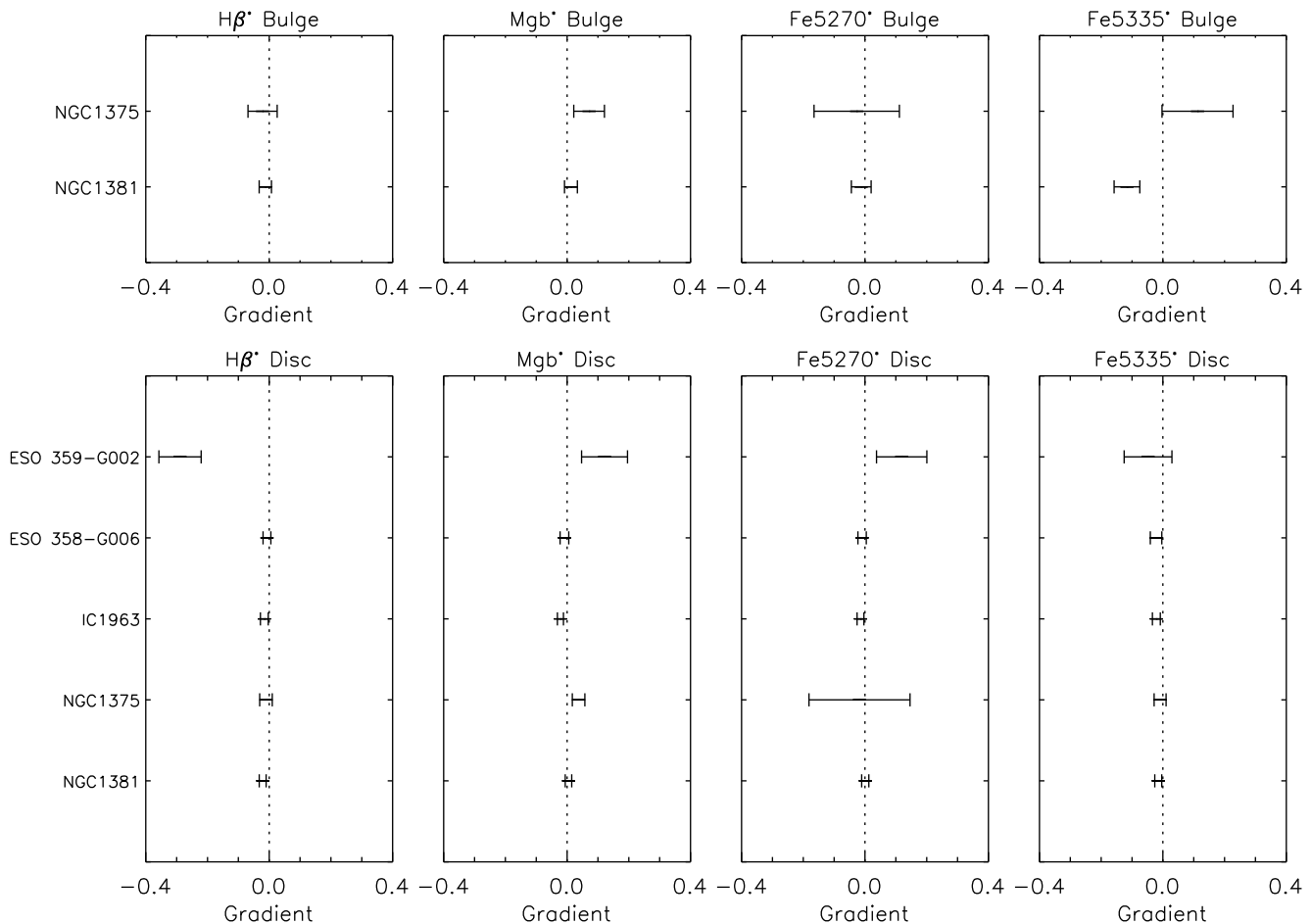


Figure 8. The line gradients for the bulge and disc in each galaxy, calculated using $\Delta \text{Index}^* / \Delta \log_{10}(R)$.

to those found in previous studies of early-type galaxies, with La Barbera & de Carvalho (2009) reporting a typical gradient of $\frac{\Delta g-r}{\Delta \log R} \sim -0.071 \pm 0.003$, Roche, Bernardi & Hyde (2010) finding a range of $-0.8 < \frac{\Delta g-r}{\Delta \log R} < 0.0$, and Suh et al. (2010) reporting values of $-0.4 < \frac{\Delta g-r}{\Delta \log R} < 0.0$. den Brok et al. (2011) similarly detected gradients within the range $-0.2 < \frac{\Delta g-i}{\Delta \log R} < 0.0$ for a sample of early-type galaxies, but found that S0s show weaker gradients than ellipticals, suggesting that the underlying mechanisms may differ.

Attempts have also been made to ascertain the causes of such gradients. For example, La Barbera & de Carvalho (2009) concluded that the main contributors to the colour gradients were the radial variations in metallicity over the galaxies, and that, while a small positive age gradient was also present, its contribution to the colour gradient was negligible in comparison. The spectral decomposition method presented here provides us with a new mechanism for seeing directly in the individual components whether these gradients are associated with changes in age or metallicity, and we now describe how this information can be exploited.

6 LINE INDEX GRADIENTS

If there were a gradient in the strength of a particular absorption line within a single component, one would expect that the scale-length

as determined within the absorption feature would differ from that of the surrounding continuum, which, in turn, would show up in the spectrum of that component generated from the best-fit model, like those shown in Fig. 2. We have therefore analysed these model spectra by calculating the Lick indices from them as a function of radius. A logarithmic gradient was then generated for each index by calculating the magnitude version of the indices,

$$\text{Index}^* = -2.5 \log_{10} \left(1 - \frac{\text{Index}}{\Delta \lambda} \right), \quad (14)$$

and measuring its variation with $\Delta \log_{10}(R)$. The resulting gradients for the bulge and disc of each galaxy are presented in Fig. 8.

Since any signal in this plot arises from a variation in the component’s scale-length at the wavelength of the index, the error on each measurement was assessed by calculating the indices that one obtains by treating the plots of scale-length versus wavelength (such as those shown in Fig. 6) as spectra, and extracting Lick indices from them: if there were a signal, then the value of scale-length in the central band should differ significantly from the value in the pseudo-continuum, leading to a non-zero index. To measure the significance of any such measurement, and hence the appropriate size of the error bars in Fig. 8, the indices measured at the true index wavelengths in plots like Fig. 6 were compared to those obtained from random locations in these plots. These results were

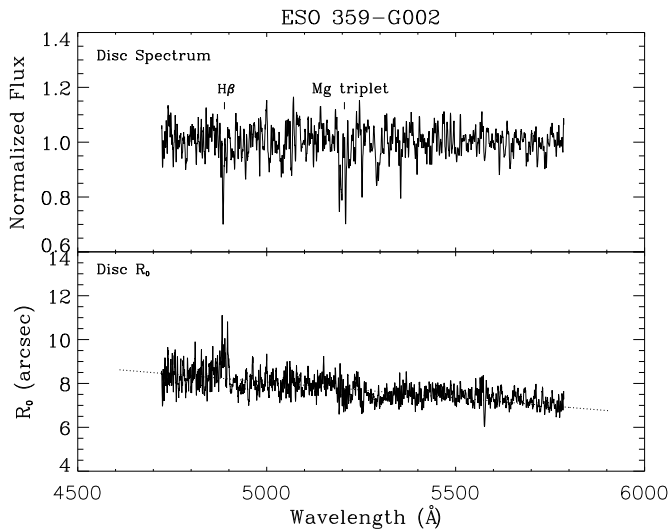


Figure 9. The decomposed disc spectrum for ESO 359-G002 (top) and a plot of its disc scale length against wavelength (bottom). A feature is present at the wavelength of the $H\beta$ line on the scale-length plot, implying that there is a gradient in its line strength.

found to be consistent with those of Bedregal et al. (2011), in which the line strength gradients were measured over the whole galaxy.

As can be seen from Fig. 8, the $H\beta$ index of ESO 359-G002 shows a gradient detected with a $> 4\sigma$ significance, which would suggest the presence of an age variation across its disc. The origins of this detection can be seen in Fig. 9, where the scale length measured at the wavelength of $H\beta$ differs from that in the surrounding continuum, just as described above. The effect of this variation on the reconstructed spectra is illustrated in Fig. 10, which shows the derived $H\beta$ feature at radii of 2 arcsec (the inner seeing limit of the galaxy) and at 8 arcsec (the disc scale length). The SSP model for this galaxy was used to translate the $H\beta$ line index gradient into an approximate age gradient of $\Delta \log_{10}(\text{age})/\Delta \log_{10}(R) \sim 1.1 \pm 0.2$. This corresponds to ages of 1.86 ± 0.14 Gyrs and 8.77 ± 0.16 Gyrs at the respective inner and outer radii shown in Fig. 10. Note, however, that such an age gradient is in the wrong sense to explain the colour gradient seen in this system.

In trying to explain the observed colour gradients, the situation is no more helpful in all the other galaxies. As is evident from Fig. 8, none of the components in any of these systems display significant gradients in any of their indices. We can translate these limits into limits on the variation in the properties of the stellar population between the centre and each component’s characteristic radius (R_e for bulges and R_0 for discs) as above. Typically, this analysis yields an upper limit of a $\sim 30\%$ change in age and metallicity between these locations. This corresponds to a colour gradient of $|\frac{\Delta(B-V)}{\Delta \log R}| \approx 0.02$ using the models of Bruzual & Charlot (2003), which cannot explain the sizable colour gradients found in Section 5. It would therefore appear that some other factor, most likely dust reddening that varies with radius, must be the underlying cause of the colour gradients.

7 DISCUSSION

We have presented a new method for analysing S0 galaxy spectra by decomposing their major-axis light into bulge and disc components on a wavelength-by-wavelength basis, in order to construct clean, high-quality spectra for each individual component. Applica-

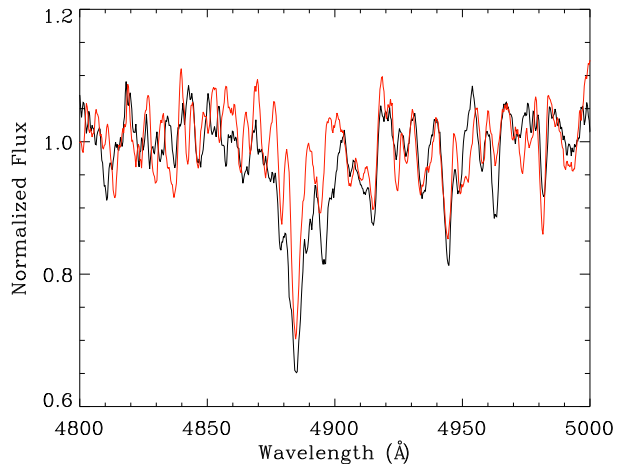


Figure 10. The $H\beta$ feature in the reconstructed spectra of the disc of ESO 359-G002 at the radii of the inner seeing limit (black), and the disc scale length (red).

tion of this method to a preliminary sample of data from the Fornax Cluster has revealed that as long as the galaxies are well-described by this two component model, and the bulge region is sufficiently resolved to allow a reliable structural fit, it is quite possible to spectrally decompose galaxies in this way.

Even this initial small sample reveals some clear systematic trends in the properties of Fornax S0s. Specifically, analysis of the Lick indices of the individual components shows that in the two galaxies that could be decomposed into two components, the bulges are systematically younger and more metal rich than the discs. This is also found to be the case more globally when comparing galaxies across the sample. Since these quantities are luminosity-weighted averages for the individual components, we cannot rule out the probability that the differences arise from relatively small amounts of late star formation, but they nonetheless point to real differences in star formation history. The positive age gradient between the bulge region and disc region has previously been documented in this data set by Bedregal et al. (2011), and has been seen in other lenticular galaxies by Fisher, Franx & Illingworth (1996), Bell & de Jong (2000), Kuntschner (2000), MacArthur et al. (2004) and Prochaska Chamberlain et al. (2011), but the new analysis technique allows us for the first time to cleanly measure the relative ages of the individual components, and also to optimise the signal-to-noise ratio of the data, and hence the precision of the measurements, by combining all of the two-dimensional spectral data into just two one-dimensional spectra.

By analysing the variation in the bulge and disc components’ scale-lengths with wavelength, we were also able to make approximate measurements of the colour gradients in the individual components, which turned out to be systematically negative, with the centre of each component redder than its outskirts. Again, such gradients have been seen before, but here for the first time we can show clearly that they exist in the individual components, not just arising from the superposition of monochromatic individual components whose relative contributions vary with radius.

By analysing any variations in the best-fit structural parameters at the wavelengths of the various Lick indices, we have further been able to measure gradients in age and metallicity. In only one galaxy was a significant age gradient detected, which interestingly was found to be in the wrong sense to explain the system’s

colour gradient. In all other components of all other galaxies, no discernable gradients were detected. The upper limits these measurements imposed were also sufficient to rule out the possibility that any of the observed colour gradients could be due to variations in the stellar population. It therefore seems likely that the red centres of all components must be attributed to centrally-concentrated dust in these systems.

Although the first results presented here already illustrate the potential power of spectroscopic bulge–disc decomposition, there are still plenty of areas for further development. One could extend the model by, for example, introducing a more general Sérsic profile instead of the de Vaucouleurs law to fit a wider range of bulge types, or one could introduce to the model additional components such as a bar, in order to see where the stellar population properties of such components fit into the developing picture of S0 galaxy formation.

It would also be helpful to apply this analysis to a somewhat larger sample obtained in a different cluster, both to improve the statistics and to search for variations between S0 properties in different locations. To this end, we are currently analysing long-slit spectra from a further sample of 21 S0 galaxies in the Virgo Cluster, and look forward to presenting the results shortly.

In addition, the method could be straight-forwardly extended to IFU data, where the effects of small scale variations, such as those due to dust lanes, can be reduced, and the star formation history throughout the two-dimensional structure can be measured more robustly. We are currently modifying this technique in order to apply it to such data.

ACKNOWLEDGEMENTS

We thank the anonymous referee for the careful reading of the manuscript, and the range of helpful suggestions. We would also like to thank Omar Almaini for his useful input to this study, and Patricia Sánchez-Blázquez for very helpful discussions and for independently testing our initial results. We would also like to thank Michele Cappellari for the use of his PPXF software. This work was based on observations made with ESO telescopes at Paranal Observatory under the program ID 070.A-0332, and was supported by STFC.

REFERENCES

- Barway S., Kembhavi A., Wadadekar Y., Ravikumar C. D., Mayya Y. D., 2007, *ApJ*, 661, L37
- Barway S., Wadadekar Y., Kembhavi A., Mayya Y. D., 2009, *MNRAS*, 394, 1991
- Beckman J., Peletier R., Knapen J., Corradi R., Gentet L., 1996, *ApJ*, 467, 175
- Bedregal A. G., Aragón-Salamanca A., Merrifield M. R., Cardiel N., 2008, *MNRAS*, 387, 660
- Bedregal A. G., Aragón-Salamanca A., Merrifield M. R., Milvang-Jensen B., 2006, *MNRAS*, 371, 1912
- Bedregal A. G., Cardiel N., Aragón-Salamanca A., Merrifield M. R., 2011, *MNRAS*, 415, 2063
- Bekki K., Shioya Y., Couch W. J., 2002, *ApJ*, 577, 651
- Bell E. F., de Jong R. S., 2000, *MNRAS*, 312, 497
- Bessell M., 1990, *PASP*, 102, 1181
- Bothun G. D., Gregg M. D., 1990, *ApJ*, 350, 73
- Bruzual G., Charlot S., 2003, *MNRAS*, 344, 1000
- Byrd G., Valtonen M., 1990, *ApJ*, 350, 89
- Caon N., Capaccioli M., D’Onofrio M. D., 1994, *A&AS*, 106, 199
- Cappellari M., Emsellem E., 2004, *PASP*, 116, 138
- Cardiel N., 2007, in *Highlights of Spanish Astrophysics IV*, Proceedings of the 7th Scientific Meeting of the Spanish Astronomical Society
- de Jong R. S., 1996, *A&A*, 313, 377
- de Vaucouleurs G., 1953, *MNRAS*, 113, 134
- den Brok M. et al., 2011, *MNRAS*, 414, 3052
- Desai V. et al., 2007, *ApJ*, 660, 1151
- Dressler A., 1980, *ApJ*, 236, 351
- Dressler A., Oemler A. J., Smail I., Barger A., Butcher H., Poggianti B. M., Sharples R. M., 1997, *ApJ*, 490, 577
- Fasano G., Poggianti B. M., Couch W. J., Bettoni D., Kjrgaard P., Moles M., 2000, *ApJ*, 452, 673
- Fisher D., Franx M., Illingworth G., 1996, *ApJ*, 459, 110
- Freeman K. C., 1970, *ApJ*, 160, 811
- González J. J., 1993, PhD thesis, Univ. California, Santa Cruz
- Gunn J. E., Gott J. R., 1972, *ApJ*, 176, 1
- Hudson M. J., Stevenson J. B., Smith R. J., Wegner G. A., Lucey J. R., Simard L., 2010, *MNRAS*, 409, 405
- Kormendy J., 1977, *ApJ*, 218, 333
- Kuntschner H., 2000, *MNRAS*, 315, 184
- La Barbera F., de Carvalho R. R., 2009, *ApJ*, 699, L76
- Larson R. B., Tinsley B. M., Caldwell C. N., 1980, *ApJ*, 237, 692
- MacArthur L. L., Courteau S., Bell E., Holtzman J. A., 2004, *ApJS*, 152, 175
- Madore B. F. et al., 1999, *ApJ*, 515, 29
- Merritt D., 1984, *ApJ*, 276, 26
- Mihos J. C., Hernquist L., 1994, *ApJ*, 425, L13
- Miller R. H., 1986, *A&A*, 167, 41
- Möllenhoff C., 2004, *A&A*, 415, 63
- Moore B., Katz N., Lake G., Dressler A., Oemler A., 1996, *Nature*, 379, 613
- Moore B., Lake G., Katz N., 1998, *ApJ*, 495, 139
- Moore B., Lake G., Quinn T., Stadel J., 1999, *MNRAS*, 304, 465
- Peletier R. F., Balcells M., 1996, *AJ*, 111, 2238
- Pompei E., Natali G., 1997, *A&AS*, 124, 129
- Prochaska Chamberlain L., Courteau S., McDonald M., Rose J., 2011, *MNRAS*, 412, 423
- Roche N., Bernardi M., Hyde J., 2010, *MNRAS*, 407, 1231
- Sánchez-Blázquez P. et al., 2006, *MNRAS*, 371, 703
- Suh H., Jeong H., Oh K., Yi S. K., Ferreras I., Schawinski K., 2010, *ApJS*, 187, 374
- Terndrup D. M., Davies R. L., Frogel J. A., DePoy D. L., Wells L. A., 1994, *ApJ*, 432, 518
- Thomas D., Maraston C., Bender R., 2003, *MNRAS*, 339, 897
- Trager S. C., Faber S. M., Worthey G., González J. J., 2000, *AJ*, 119, 1645
- Varela J., Moles M., Márquez I., Galletta G., Masegosa J., Bettoni D., 2004, *A&A*, 420, 873
- Vazdekis A., Sánchez-Blázquez P., Falcón-Barroso J., Cenarro A. J., Beasley M. A., Cardiel N., Gorgas J., Peletier R. F., 2010, *MNRAS*, 404, 1639
- Whitmore B. C., Gilmore D. M., Jones C., 1993, *ApJ*, 407, 489
- Worthey G., Faber S. M., González J. J., Burstein D., 1994, *ApJS*, 94, 687
- Worthey G., Ottaviani D. L., 1997, *ApJS*, 111, 377

APPENDIX A: TABLES

In this appendix we include tables with different parameters for each galaxy in the sample. Only NGC 1381 and NGC 1375 could be decomposed into bulge and disc components, IC 1963, ESO 358-G006 and ESO 359-G002 gave disc only fits, and NGC 1316, NGC 1380, NGC 1380A and ESO 358-G059 could not be fitted with the current model. The errors are presented in parentheses next to the values, and represent one sigma uncertainties in the measurements. The results for R_e , R_0 , V_{LOS} and σ are given for both halves of the major axis in each case, where V_{LOS} and σ are the line-of-sight velocity and velocity dispersions after the corrections described in Section 3.

Name	M_B	R_e [arcsec]	R_0 [arcsec]	σ_0 [km s ⁻¹]	V_{LOS} [km s ⁻¹]
(1)	(2)	(3)	(4)	(5)	(6)
NGC1381	−19.1 (0.1)	6.7 (0.2)	25.1 (0.2)	150.5 (12.6)	1718.5 (8.8)
		7.5 (0.2)	26.4 (0.3)	157.9 (14.0)	1715.0 (9.0)
NGC1375	−18.2 (0.2)	5.0 (0.4)	16.4 (0.3)	115.0 (9.9)	785.2 (6.6)
		3.5 (0.4)	16.8 (0.5)	116.5 (9.4)	778.3 (6.5)
IC1963	−18.5 (0.1)	–	15.5 (0.3)	59.0 (2.3)	1635.5 (1.7)
		–	15.0 (0.3)	61.8(1.8)	1631.7 (1.6)
ESO 358-G006	−17.5 (0.2)	–	10.5 (0.2)	98.8 (5.7)	1264.2 (4.3)
		–	10.4 (0.2)	99.6 (6.4)	1258.5 (4.7)
ESO 359-G002	−17.3 (0.2)	–	7.3 (0.5)	58.9 (3.3)	1439.7 (2.5)
		–	7.4 (0.5)	62.7 (3.2)	1457.3 (2.6)
NGC 1316	−22.3 (0.1)	–	–	–	–
NGC 1380	−20.6 (0.1)	–	–	–	–
NGC 1380A	−18.1 (0.2)	–	–	–	–
ESO 358-G059	−17.4 (0.2)	–	–	–	–

Note. Column (2): absolute magnitude in B-band according to Madore et al. (1999); Column (3): bulge effective radius, measured at the central wavelength of the V-band filter (5510 Å); Column (4): disc scale length, measured at the central wavelength of the V-band filter (5510 Å); Column (5): velocity dispersion; Column (6): line-of-sight velocity.